

Spherical polytropic balls cannot mimic black holes

Hiromi Saida

Department of Physics, Daido University, Minami-ku, 457-8530 Nagoya, Japan

E-mail: saida@daido-it.ac.jp

Atsuhito Fujisawa, Chul-Moon Yoo and Yasusada Nambu

Department of Physics, Nagoya University, Chikusa-ku, 464-8602 Nagoya, Japan

E-mail: fujisawa@gravity.phys.nagoya-u.ac.jp

E-mail: yoo@gravity.phys.nagoya-u.ac.jp

E-mail: nambu@gravity.phys.nagoya-u.ac.jp

Abstract. The so-called black hole shadow is a dark region which is expected to appear in a fine image of optical observation of black holes. It is essentially an absorption cross section of black hole, and the boundary of shadow is determined by unstable circular orbits of photons (UCOP). If there exists a compact object possessing UCOP but no black hole horizon, it can provide us with the same shadow image with black holes, and a detection of shadow image cannot be a direct evidence of black hole existence. However, we show that a static spherical polytropic ball of perfect fluid cannot possess UCOP, if the sound speed at centre is subluminal (slower-than-light). This implies that, if the polytrope is a good model of stellar matter in compact objects, a detection of shadow image is regarded as a good evidence of black hole existence. As a by-product, we have found an upper bound of mass-to-radius ratio of polytropic ball, $M_*/R_* < 0.281$, under the subluminal sound speed condition.

PACS numbers: 04.40.-b , 95.30.Sf , 97.60.Lf

Submitted to: *Class. Quantum Grav.*

1. Introduction

In recent years, the resolution of image by very-long-baseline-interferometer (VLBI) radio observation is approaching to the visible angular size of SgrA*, about 10 micro-arcsecond (black hole of $4 \times 10^6 M_\odot$ is at 8 kpc), which is the largest visible angular size in known black hole candidates [1, 2]. The so-called black hole shadow is expected to be resolved by such fine observation near future (see [3, 4] and references therein). It seems to be currently a common understanding that seeing the black hole shadow is believing the existence of black hole horizon.

However, this common understanding has not been confirmed in general relativity as follows: Remember that the black hole shadow is a dark region appearing in an optical image of black holes, on which some photons would be detected if the black hole did not exist. Therefore, the shadow is essentially an absorption cross section of black hole. However, it should be emphasized that photons on the edge of shadow have been circulating around black hole before coming to the observer. The innermost circular orbit of those photons is not a great circle on black hole horizon, but an unstable circular orbit of photons (UCOP). That is to say, the boundary of shadow is determined not by black hole horizon, but by UCOP. This indicates that the direct origin of shadow is UCOP, not black hole horizon. Hence, although we can conclude the existence of UCOP once a shadow is observed, however, we cannot conclude immediately the existence of black hole horizon even if a shadow is clearly observed.

Here, let us assign a term, black hole mimicker, to a compact object possessing UCOP but no black hole horizon. If there exists a black hole mimicker, it can provide us with the same shadow image with black holes in optical observation, and a detection of shadow image cannot be a direct evidence of black hole existence. Therefore, we are interested in an existence/non-existence condition of black hole mimickers.

Some exotic candidates of black hole mimicker have been proposed, such as gravastars and boson stars. The gravastar as a black hole mimicker and its shadow image have been examined [5], whereas the others remain to be examined. Those exotic models may be interesting. However, we focus on a rather usual model in this paper.

Consider a static spherical ball of perfect fluid, which connects to Schwarzschild geometry at surface. A fluid ball, which does not possess black hole horizon, becomes a black hole mimicker if it possesses one of following properties:

- (A) A fluid ball is so compact that there appears an UCOP in the outside Schwarzschild geometry.
- (B) A fluid ball is not so compact as case (A), but an UCOP exists inside the ball.

For case (A), if the surface of fluid ball neither emit nor reflect any radiation, this ball can provide us with the same shadow image with a black hole. For case (B), if the fluid outside UCOP is completely transparent and if the fluid inside UCOP is not transparent, this ball can provide us with the same shadow image with a black hole.

Concerning the case (A), a mass-to-radius ratio M_*/R_* of fluid ball is interesting, where M_* and R_* are respectively the total mass and surface radius of the ball measured

in the dimension of length. In order to avoid gravitational collapse, an inequality, $M_*/R_* < 1/2$, must hold. Further, a lower upper bound has been found by the previous work [6] as

$$\frac{M_*}{R_*} \leq 0.363761 \quad \Leftrightarrow \quad 2.749057M_* \leq R_*, \quad (1)$$

where three conditions are assumed; non-increasing mass density in outward direction, barotropic form of equation of states, and subluminal (slower-than-light) condition of sound speed. Since the lower bound of radius R_* is less than $3M_*$ which is the radius of UCOP in outside Schwarzschild geometry, there remains a possibility that a black hole mimicker of case (A) exists. On the other hand, concerning the case (B), there is no existing work analyzing UCOP inside a matter as far as we know.

In this paper, a polytropic equation of states is considered, which is a representative example of barotropic equation of states. We examine whether or not the cases (A) and (B) are possible for polytropic spherical ball. Our result is that there cannot exist UCOP in neither outside nor inside of polytropic fluid ball, if the sound speed at centre is subluminal. This implies that, if the polytrope is a good model of stellar matter in compact objects, a detection of shadow image is regarded as a good evidence of existence of black hole.

In section 2, a set-up of our analysis is described. Sections 3 and 4 are devoted to analyses of, respectively, cases (A) and (B). Section 5 is for summary and discussions.

2. Static spherical polytropic ball

We consider static spherical ball made of polytropic perfect fluid. The metric of this spacetime is given by a line element,

$$ds^2 = g_{\mu\nu} dx^\mu dx^\nu = -e^{2\Phi(r)} c^2 dt^2 + \frac{dr^2}{1 - 2Gm(r)/(c^2 r)} + r^2(d\theta^2 + \sin^2\theta d\varphi^2), \quad (2)$$

where (t, r, θ, φ) is spherical polar coordinates, $\Phi(r)$ gives a lapse function, and $m(r)$ is a mass of fluid contained in spherical region of radius r . The stress-energy-momentum tensor of perfect fluid is $T_{\mu\nu} = [\sigma(r)c^2 + p(r)]u_\mu u_\nu + p(r)g_{\mu\nu}$, where $u = e^{-\Phi}\partial_{ct}$ is a four-velocity of static fluid, and $\sigma(r)$ and $p(r)$ are respectively a mass density and pressure of fluid.

A condition, $m(0) = 0$, should hold due to the regularity of spacetime at centre. This implies a finite mass density at centre, $\sigma_c = \sigma(0) \neq \infty$, where a suffix c denotes the value at centre. We normalize all quantities by σ_c ,

$$R := \frac{\sqrt{G\sigma_c}}{c} r, \quad \Sigma(R) := \frac{\sigma(r)}{\sigma_c}, \quad M(R) := \frac{\sqrt{G^3\sigma_c}}{c^3} m(r), \quad P(R) := \frac{p(r)}{\sigma_c c^2}. \quad (3)$$

These are dimension-less. The lapse function, $\Phi(r) := \Phi(R)$, does not need normalization because Φ is originally dimension-less by definition (2).

Barotropic class of equation of states is expressed as $P = P(\Sigma)$. We consider a representative example in this class, which is called the polytrope,

$$P(\Sigma) = K\Sigma^{1+1/n}, \quad (4a)$$

where K and n are positive constants, and n is called the polytropic index. By normalization (3), the mass density at centre is unity, $\Sigma_c = 1$. Therefore, the coefficient K is equal to a pressure at centre in our normalization (3),

$$P_c = K (= P(\Sigma = 1)). \quad (4b)$$

The surface of static spherical fluid ball is defined by vanishing pressure, $P_* = 0$, where a suffix $*$ denotes the value at surface. Therefore, the mass density at surface is zero due to polytropic equation of states (4a), $\Sigma_* = 0$. The normalized mass density takes values in the interval,

$$(\Sigma_* =) 0 \leq \Sigma \leq 1 (= \Sigma_c). \quad (5)$$

Regarding Σ as an independent variable, this finite interval of Σ seems to be useful for numerical analysis. Hence, we regard all variables as functions of Σ ,

$$R = R(\Sigma) \quad , \quad M = M(\Sigma) \quad , \quad \Phi = \Phi(\Sigma), \quad (6)$$

and $P(\Sigma)$ is already expressed as a function of Σ in (4a). The surface radius R_* and total mass M_* of polytropic ball are determined by

$$R_* = R(\Sigma = 0) \quad , \quad M_* = M(\Sigma = 0). \quad (7)$$

The sound speed V in polytropic ball is given by

$$V^2 = \frac{dP(\Sigma)}{d\Sigma} = P_c \left(1 + \frac{1}{n}\right) \Sigma^{1+1/n}. \quad (8)$$

This sound speed is normalized by light speed. Obviously, this V decreases from centre ($\Sigma_c = 1$) to surface ($\Sigma_* = 0$). The highest sound speed is given at centre,

$$V_c^2 = P_c \left(1 + \frac{1}{n}\right). \quad (9)$$

In this paper, we assume a subluminal condition of sound speed,

$$V_c \leq 1. \quad (10)$$

The outside region of polytropic ball, $R > R_*$, is described by Schwarzschild geometry of mass M_* . The inside region $R \leq R_*$ is determined by Einstein equation and conservation law $T^{\mu\nu}{}_{;\nu} = 0$, which are reduced to the Tolman-Oppenheimer-Volkoff (TOV) equations,

$$\frac{dM}{d\Sigma} = 4\pi R^2 \Sigma \frac{dR}{d\Sigma} \quad (11a)$$

$$\frac{dP}{d\Sigma} = - \frac{(\Sigma + P)(M + 4\pi R^3 P)}{R(R - 2M)} \frac{dR}{d\Sigma} \quad (11b)$$

$$\frac{d\Phi}{d\Sigma} = - \frac{1}{\Sigma + P} \frac{dP}{d\Sigma}. \quad (11c)$$

Two functions $R(\Sigma)$ and $M(\Sigma)$ are obtained by solving (11a) and (11b) under the equation of states (4a). Substituting those solutions into (11c), $\Phi(\Sigma)$ is obtained. Those solutions of TOV equations depend on two parameters, V_c and n .

Under the set-up given above, our aim is to analyze the problem, whether or not the properties (A) and (B), which are described in section 1, hold for polytropic ball under

the subluminal-sound-speed condition (10). In following analyses, TOV equations (11a) and (11b) are solved numerically. A technical remark for numerical calculation is summarized in Appendix A, which is applied to both sections 3 and 4. All of our numerical analyses are performed with Mathematica ver.10.

3. Problem A: Can an UCOP appear outside a polytropic ball?

The problem in this section is whether or not an inequality, $R_* < 3M_*$, holds for polytropic balls under the condition (10). If $R_* < 3M_*$, then an UCOP appears outside a polytropic ball. Otherwise, if $3M_* < R_*$, an UCOP does not appear outside the ball. Our strategy is as follows:

- A1:** Solve numerically TOV equations (11a) and (11b) for given values of parameters (V_c, n) , and calculate the mass-to-radius ratio, $3M_*/R_*$.
- A2:** Iterate the step A1 with varying parameters (V_c, n) , so as to obtain the ratio, $3M_*/R_*$, as a function of parameters (V_c, n) , $3M_*/R_*(V_c, n)$
- A3:** Find the maximum value of $3M_*/R_*(V_c, n)$.[‡] If the maximum is less than unity, we conclude that the inequality, $3M_* < R_*$, holds for all values of (V_c, n) , and no UCOP appears outside the polytropic balls under subluminal-sound-speed condition.

In Newton gravity, the total mass and surface radius of polytropic ball are finite in the interval of index, $0 < n < 5$, but diverge in the interval, $5 \leq n$, for any value of $V_c > 0$. However, in Einstein gravity, Nilsson and Uggla [7] have found numerically a complicated situation about behaviours of M_* and R_* in a half-infinite interval of central sound speed, $0 < V_c$:

- In the interval of polytropic index, $0 < n < 3.339$, both of M_* and R_* are finite.
- In the interval, $3.339 \leq n < 5$, a complicated behaviour is found.
 - Both of M_* and R_* are finite for almost of all values of (V_c, n) in the present parameter region.
 - However, both of M_* and R_* diverge at some discrete points $(V_c^{(i)}, n^{(i)})$ in V_c - n plane, where $i = 1, 2, \dots, N_{\text{div}}$. The number of such divergence points, N_{div} (= finite or countable infinity), cannot be read from Nilsson-Uggla [7].

Note that, although the existence of some divergence points $(V_c^{(i)}, n^{(i)})$ has been definitely confirmed, the accurate positions of them have not been specified.[§]

- In the interval, $5 \leq n$, both of M_* and R_* are infinity.

Note that the mass-to-radius ratio has not been analyzed in Nilsson-Uggla [7]. The analysis of the ratio is our task.

[‡] Note that the mass-to-radius ratio is bounded above as mentioned at (1). Therefore, a maximum value of $3M_*/R_*$, under the condition (10), is to be obtained by our numerical analysis.

[§] Two examples of such divergence points are $(V_c, n) = (V_c^{(1)}, 3.357)$, $(V_c^{(2)}, 4.414)$, where the values $V_c^{(1)}$ and $V_c^{(2)}$ cannot be read from Nilsson-Uggla [7].

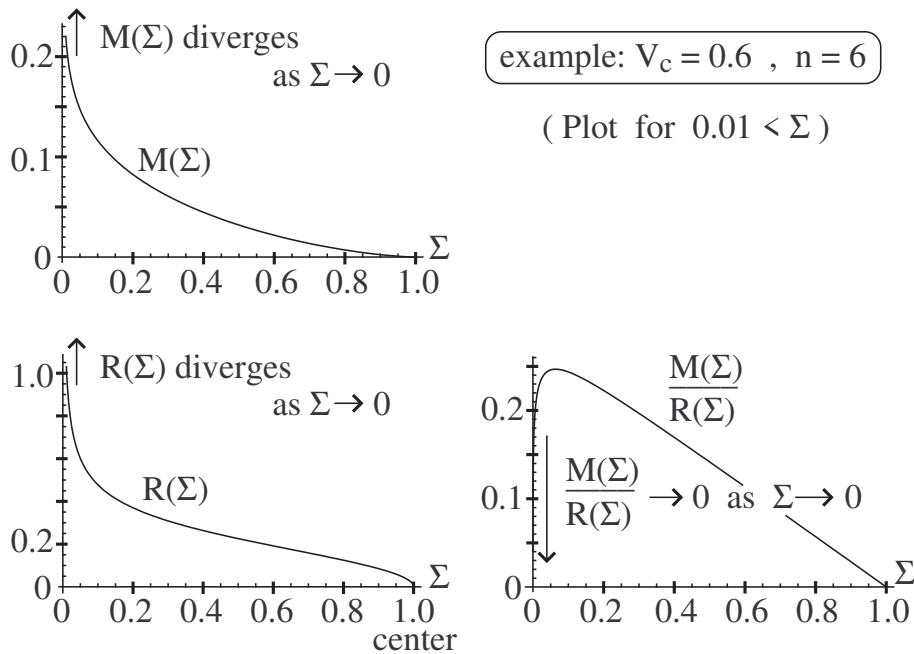


Figure 1. Numerical solution of TOV equations at $(V_c, n) = (0.6, 6)$. Although M_* and R_* are infinity, the mass-to-radius ratio M_*/R_* becomes zero.

From the above behaviour of M_* and R_* found by Nilsson-Uggla, a physically interesting region of parameters are

$$0 < V_c \leq 1 \quad , \quad 0 < n < 5, \quad (12)$$

where the interval of V_c is the subluminal-sound-speed condition (10). It is enough for our aim to calculate the ratio, $3M_*/R_*$, in this parameter region. However, the parameter points $(V_c^{(i)}, n^{(i)})$, where M_* and R_* diverge in the region (12), may not be included in the grid points of numerical analysis (see the step A2 of our strategy). In order to guess a behaviour of $3M_*/R_*$ at those points $(V_c^{(i)}, n^{(i)})$, we observe the solutions of TOV equations in the interval, $5 \leq n$, where M_* and R_* diverge as well. Figure 1 is an example with $V_c = 0.6$ and $n = 6$. This figure shows that, although the mass $M(\Sigma)$ and radius $R(\Sigma)$ diverge as the surface ($\Sigma = 0$) is approached, the mass-to-radius ratio $M(\Sigma)/R(\Sigma)$ converges to zero. The same behaviour is observed for the other values of (V_c, n) in the interval, $5 \leq n$. Hence, it is expected, even at the parameter points $(V_c^{(i)}, n^{(i)})$ where M_* and R_* diverge in the region (12), the mass-to-radius ratio converges to zero.

With the help of above discussion, we can safely carry out our strategy of numerical analysis, composed of steps A1, A2 and A3. The result is shown in figure 2, in which the contours of $3M_*/R_*$ are plotted. Although our main interest is in the parameter region (12), we have calculated for a bit larger region, $0.05 \leq V_c \leq 1.5$ and

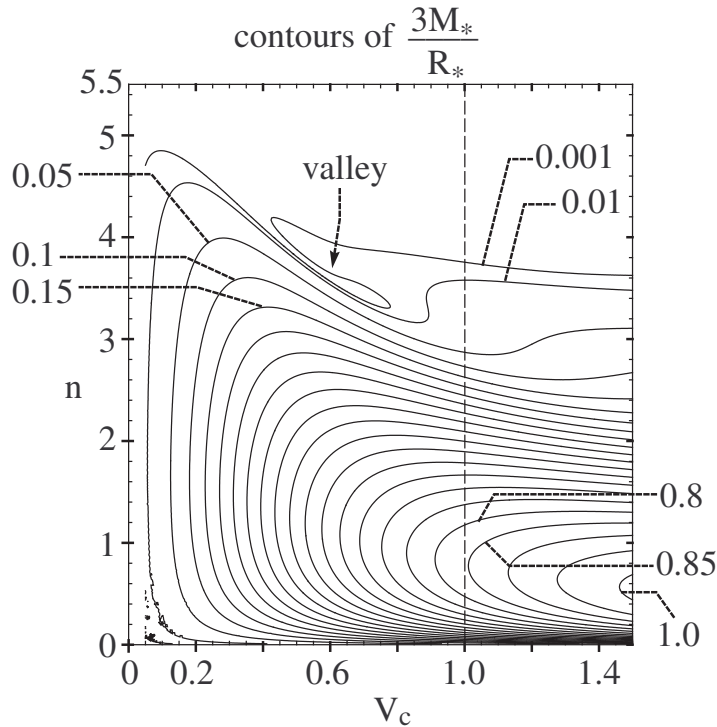


Figure 2. Contours of $3M_*/R_*$ on V_c - n plane. Numerical calculation is performed in the region, $0.05 \leq V_c \leq 1.5$ and $0.01 \leq n \leq 5.5$. Obviously, the inequality, $3M_*/R_* < 1$, holds under the subluminal-sound-speed condition, $V_c \leq 1$. For small values of V_c and n , numerical errors become manifest.

$0.01 \leq n \leq 5.5$. || It is obvious that the maximum value of $3M_*/R_*$ in the region (12) appears on the vertical line at $V_c = 1$ in figure 2. This maximum takes the value between $3M_*/R_* = 0.8$ and 0.85 . (A more precise value is calculated in section 5.) Hence, we can conclude that the inequality, $3M_*/R_* < 1$, holds in the physically interesting region (12). No UCOP appears in the outside Schwarzschild geometry under the subluminal-sound-speed condition (10).

4. Problem B: Can an UCOP appear inside a polytropic ball?

The problem in this section is whether an UCOP can exist inside a polytropic ball under the subluminal-sound-speed condition (10). For the first, a feature of UCOP in static spherical spacetimes is summarized. Next, it is applied to the polytropic ball, and shown that no UCOP can exist inside a polytropic ball.

|| In figure 2, the ratio $3M_*/R_*$ is small enough in the interval, $5 \leq n \leq 5.5$. This is consistent with the figure 1 and discussion after (12). Further, we have found numerical implications, although details are not shown here, that the points $(V_c^{(i)}, n^{(i)})$, where M_* and R_* diverge in the region (12), form a line along the valley shown in figure 2, and this line seems to approach $(V_c, n) = (0, 5)$.

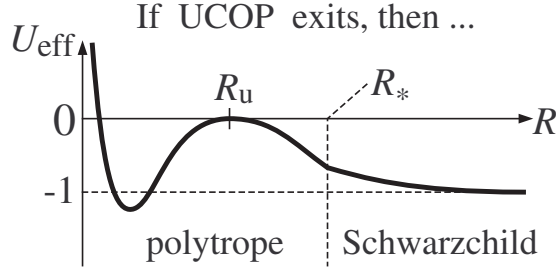


Figure 3. A schematic graph of $U_{\text{eff}}(R)$ if an UCOP exists inside a polytropic ball.

4.1. UCOP in static spherical spacetimes

The feature of UCOP in the static spherical spacetime of metric (2) is determined by null geodesic equation. Denoting an affine parameter and radial coordinate of null geodesic by, respectively, λ and $R_{\text{null}}(\lambda)$ under the normalization (3), the radial component of null geodesic equation on spacetime (2) is

$$\frac{dR_{\text{null}}}{d\lambda} + \omega^2 U_{\text{eff}}(R_{\text{null}}) = 0, \quad (13)$$

where U_{eff} is the effective potential given by

$$U_{\text{eff}}(R) = \left[\frac{b^2}{R^2} - \exp(-2\Phi(R)) \right] \left(1 - \frac{2M(R)}{R} \right), \quad b = \frac{l}{\omega}, \quad (14)$$

where $M(R)$ and $\Phi(R)$ are regarded as functions of R given by solving TOV equations, b is an impact parameter, and l and ω are respectively orbital angular momentum and frequency of photon measured at infinity.

A photon propagating on an UCOP remains at constant radius ($dR_{\text{null}}/d\lambda = 0$), but it is unstable. Hence, the radius of UCOP, R_u , is determined by following conditions,

$$U_{\text{eff}}(R_u) = 0 \quad , \quad \frac{dU_{\text{eff}}}{dR}(R_u) = 0 \quad , \quad \frac{d^2U_{\text{eff}}}{dR^2}(R_u) \leq 0. \quad (15)$$

This implies that, if an UCOP exists inside a polytropic ball, the top of potential barrier touches below the zero level at R_u as shown in figure 3.

By substituting (14) into (15), we obtain

$$\frac{2}{R_u} F(R_u) - \frac{dF}{dR}(R_u) = 0 \quad (16a)$$

$$\frac{1}{R_u} \frac{dF}{dR}(R_u) - \frac{d^2F}{dR^2}(R_u) \geq 0 \quad (16b)$$

$$b^2 = \frac{R_u^2}{F(R_u)}, \quad (16c)$$

where

$$F(R) := \exp(2\Phi(R)) \quad (= -g_{00}). \quad (17)$$

The radius of UCOP, R_u , is determined by (16a) and (16b), and then the impact parameter of null geodesic circulating on UCOP forever is obtained by (16c). Therefore,

the existence condition of UCOP consists of two parts; an algebraic equation (16a) and an inequality (16b), which do not include the impact parameter.

4.2. Non-existence of UCOP inside the polytropic balls

In order to apply the existence conditions of UCOP (16a) and (16b) to polytropic balls, we need a concrete functional form of $\Phi(\Sigma) = (1/2) \ln F(\Sigma)$. Substituting the equation of states (4a) into a TOV equation (11c),

$$\frac{d\Phi(\Sigma)}{d\Sigma} = -\left(1 + \frac{1}{n}\right) \frac{P_c \Sigma^{1/n-1}}{1 + P_c \Sigma^{1/n}} = -(n+1) \frac{d \ln(1 + P_c \Sigma^{1/n})}{d\Sigma}. \quad (18)$$

Integration constant is determined by a junction condition of metric at the surface of polytropic ball, $\exp(2\Phi_*) = 1 - 2M_*/R_*$. We obtain

$$F(\Sigma) = e^{2\Phi(\Sigma)} = \frac{F_*}{(1 + P_c \Sigma^{1/n})^{2(n+1)}} = F_* \left(1 + \frac{P(\Sigma)}{\Sigma}\right)^{-2(n+1)}, \quad (19)$$

where $F_* = 1 - 2M_*/R_*$. Regarding Σ as a function of R , which is given by solving TOV equations (11a) and (11b), we obtain F as a function of R , $F(R)$.

From (19), first and second differentials of $F(R)$ are calculated,

$$\begin{aligned} \frac{dF(R)}{dR} &= 2 \frac{M + 4\pi R^3 P}{R(R - 2M)} F(R) \quad (> 0) \\ \frac{d^2F(R)}{dR^2} &= \frac{1}{R} \left[\frac{4M - R}{R - 2M} + 4\pi R^3 \left(\frac{\Sigma + P}{R - 2M} + \frac{\Sigma + 3P}{M + 4\pi R^3 P} \right) \right] \frac{dF(R)}{dR}, \end{aligned} \quad (20)$$

where TOV equations (11a), (11b) and (11c) are used. Substituting these differentials into the existence conditions of UCOP (16a) and (16b), we obtain

$$C_1|_{R=R_u} = 0 \quad , \quad C_2|_{R=R_u} \geq 0, \quad (21)$$

where

$$\begin{aligned} C_1 &= R - 4\pi R^3 P - 3M \\ C_2 &= 1 - \left[\frac{4M - R}{R - 2M} + 4\pi R^3 \left(\frac{\Sigma + P}{R - 2M} + \frac{\Sigma + 3P}{M + 4\pi R^3 P} \right) \right]. \end{aligned} \quad (22)$$

If there does not exist R_u which satisfies the conditions (21) for any value of parameters (V_c, n) in the physically interesting region (12), then it is concluded that no UCOP can appear inside the polytropic balls.

Note that the value of quantities C_1 and C_2 are calculated by substituting the solutions of TOV equations (11a) and (11b). The solutions of TOV equations are functions of Σ and depend on parameters (V_c, n) . Hence, in our analysis, C_1 and C_2 can be obtained numerically as functions of three arguments, $C_1(\Sigma, V_c, n)$ and $C_2(\Sigma, V_c, n)$. Then, in order to check whether or not there exists R_u satisfying (21), our strategy is as follows:

B1: Solve numerically TOV equations (11a) and (11b) for given value of parameters (V_c, n) , and iterate this numerical calculation with varying V_c and fixing n at a given value. This iteration produces $C_1(\Sigma, V_c, n)$ and $C_2(\Sigma, V_c, n)$ as functions of (Σ, V_c) for the given value of n .

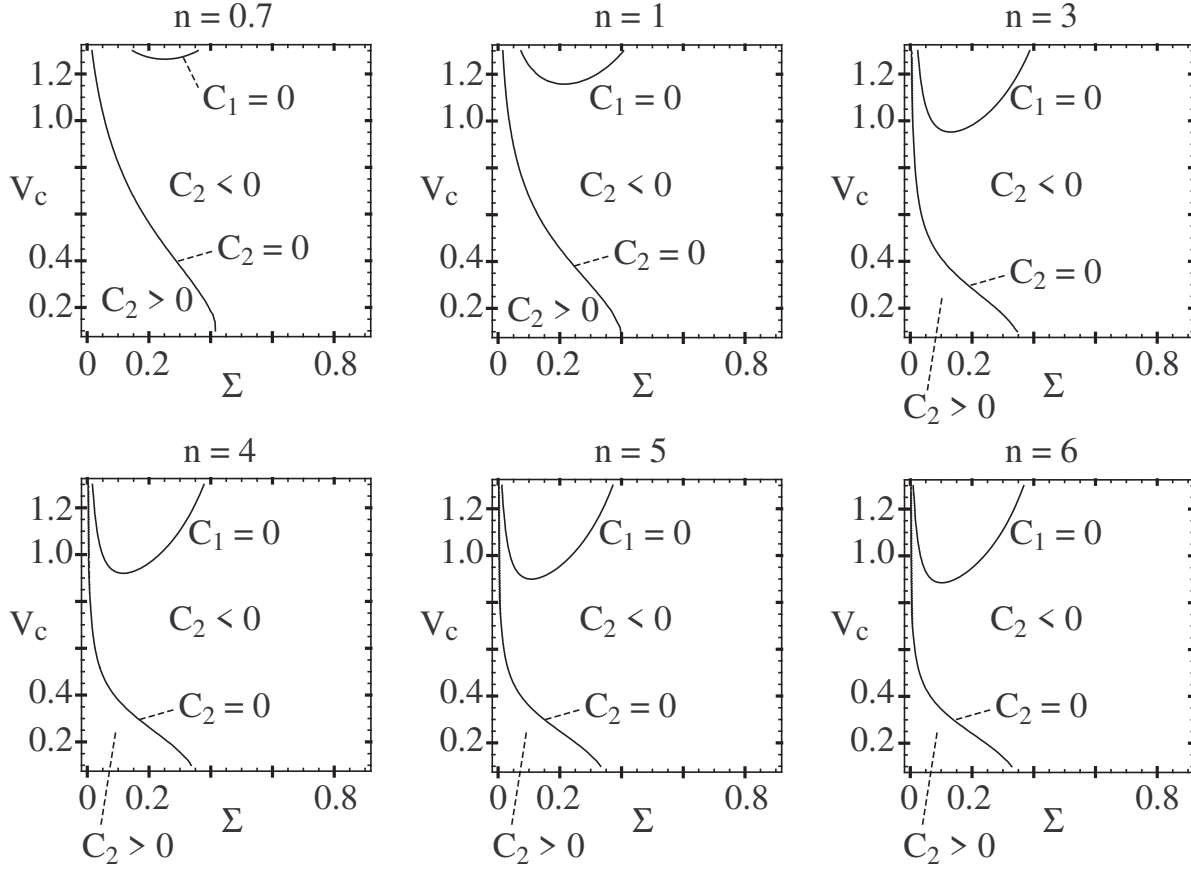


Figure 4. Plots of curves $C_1(\Sigma, V_c, n) = 0$ and $C_2(\Sigma, V_c, n) = 0$ in Σ - V_c plane for some fixed n . The regions, $C_2 > 0$ and $C_2 < 0$, are also denoted. It is recognized that the existence conditions of UCOP (21) are not satisfied.

B2: Plot two curves, $C_1 = 0$ and $C_2 = 0$, and identify two regions, $C_2 > 0$ and $C_2 < 0$, in Σ - V_c plane for the given n . If the curve $C_1 = 0$ does not intersect with the region $C_2 \geq 0$, it is concluded that no UCOP exists inside the polytropic ball of given value of n .

B3: Iterate the steps B1 and B2 with varying n , and check whether or not the intersection of $C_1 = 0$ with $C_2 \geq 0$ exists at each value of n . If the intersection does not appear for any value of n , then we conclude that an UCOP can never appear inside the polytropic balls.

The numerical result of this strategy is shown in figure 4. We find that the curve $C_1 = 0$ remains in the region $C_2 < 0$ for all values of $n = 0.7, 1, 3, 4, 5, 6$. The same feature is found for the other values of n as far as we have calculated. Hence, no UCOP appears inside the polytropic ball. Furthermore, the non-existence of UCOP inside polytropic balls seems to hold for not only the physically interesting parameter region (12) but also all parameter region, $0 < n$ and $0 < V_c$.

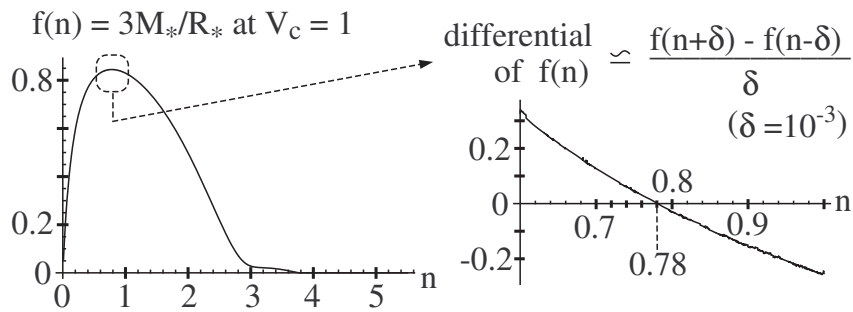


Figure 5. Sectioned diagram of figure 2 at $V_c = 1$. $f(n)$ describes $3M_*/R_*$ as a function of n at $V_c = 1$. Differential of $f(n)$ is plotted by an approximation, $df(n)/dn \simeq [f(n+\delta) - f(n-\delta)]/\delta$, where $\delta = 10^{-3}$.

5. Summary and discussions

We have investigated whether or not an UCOP can exist in the spacetime of static spherical polytropic ball. By numerical analyses of TOV equations and null geodesic equation, our conclusion is the non-existence of UCOP in neither inside nor outside of the polytropic ball under the subluminal-sound-speed condition. That is to say, polytropic balls cannot be a black hole mimicker which possesses UCOP but no black hole horizon. This implies that, if the polytrope is a good model of stellar matter in compact objects, a detection of shadow image by optical observation is regarded as a good evidence of existence of black hole.

Finally, let us discuss a by-product of our analysis. In section 3, the ratio of total mass to surface radius of polytropic ball, M_*/R_* , has been the central issue. As mentioned at (1), the mass-to-radius ratio must be bounded above, $M_*/R_* < 1/2$, in order to avoid gravitational collapse. Buchdahl [8] decreased the upper bound to, $M_*/R_* < 4/9$, with assuming non-increasing mass density in outward direction and barotropic equation of states. Next, Barraco and Hamity [9] decreased the Buchdahl's upper bound to, $M_*/R_* < 3/8$, by adding dominant energy condition to Buchdahl's assumptions. Furthermore, in our previous work [6], we decreased the Barraco-Hamity's upper bound as shown in (1) by replacing the dominant energy condition with subluminal-sound-speed condition. All these upper bound remained greater than $1/3$, which permits the existence of black hole mimicker. However, as shown in figure 2 of this paper, the upper bound of M_*/R_* is decreased to a value lower than $1/3$, by restricting the equation of states to polytrope (4a). Since the upper bound is found on the vertical line at $V_c = 1$ in figure 2, a sectioned diagram of figure 2 at $V_c = 1$ is useful to read a precise value of the upper bound. It is shown in figure 5, where we define $f(n)$ by $3M_*/R_*$ as a function of n at $V_c = 1$. From this figure, it is concluded that the following inequality holds in the physically interesting parameter region (12),

$$\frac{3M_*}{R_*} < 0.844 \quad \left(\Leftrightarrow \frac{M_*}{R_*} < 0.281 \right), \quad (23)$$

where the upper bound is given by parameters $V_c = 1$ and $n \simeq 0.78$, and the value of upper bound is numerically calculated, $f(0.78) \simeq 0.844$.

Acknowledgments

H.S. was supported by Japan Society for the Promotion of Science (JSPS), Grant-in-Aid for Scientific Research (KAKENHI, Exploratory Research, 26610050).

Appendix A. On numerical treatment of TOV equations

Right-hand sides of TOV equations (11a) and (11b) are indeterminate form at centre because of the conditions, $M \rightarrow 0$ and $R \rightarrow 0$ as $\Sigma \rightarrow 1$. Therefore, in solving TOV equations numerically, we have made use of perturbative solutions near the centre.

In order to consider a perturbation near centre, we regard the radius R as an independent variable, and the mass density as a function of radius, $\Sigma(R)$. TOV equations (11a) and (11b) are rearranged to

$$\begin{aligned} \frac{dM(R)}{dR} &= 4\pi R^2 \Sigma(R) \\ \frac{dP(R)}{dR} &= -\frac{[\Sigma(R) + P(R)][M(R) + 4\pi R^3 P(R)]}{R[R - 2M(R)]}. \end{aligned} \quad (\text{A.1})$$

For a sufficiently small radius $R \ll 1$, we introduce perturbations,

$$\begin{aligned} M(R) &= M_{(1)}R + M_{(2)}R^2 + M_{(3)}R^3 + \dots \\ P(R) &= P_c + P_{(1)}R + P_{(2)}R^2 + P_{(3)}R^3 + \dots \\ \Sigma(R) &= 1 + \Sigma_{(1)}R + \Sigma_{(2)}R^2 + \Sigma_{(3)}R^3 + \dots, \end{aligned} \quad (\text{A.2})$$

where conditions $M(R=0) = 0$, $\Sigma(R=0) = 1$ and $P(R=0) = P_c$ are included. Substituting (A.2) into (A.1), we obtain $M_{(1)} = 0$, $M_2 = 0$, $P_{(1)} = 0$ and remaining parts,

$$\begin{aligned} M(R) &= \frac{4}{3}\pi R^3 + \pi \Sigma_{(1)} R^4 + \dots \\ P(R) &= P_c - \frac{2}{3}\pi(1 + 3P_c)(1 + P_c)R^2 - \frac{\pi}{9}(7 + 15P_c)\Sigma_{(1)}R^3 + \dots \\ \Sigma(R) &= 1 + \Sigma_{(1)}R + \Sigma_{(2)}R^2 + \Sigma_{(3)}R^3 + \dots, \end{aligned} \quad (\text{A.3})$$

where the central pressure P_c and coefficients $\Sigma_{(n)}$ ($n = 1, 2, 3, \dots$) are determined by concrete form of equation of states.

Substitute these perturbative expansions into the equation of states (4a), we obtain

$$\Sigma_{(1)} = 0 \quad , \quad \Sigma_{(2)} = -\frac{n}{n+1} \frac{2\pi(1 + P_c)(1 + 3P_c)}{3P_c}. \quad (\text{A.4})$$

Hence, denoting a small radius by $R_\delta \ll 1$, the mass density Σ_δ and mass M_δ at $R = R_\delta$ are approximately given by $\Sigma_\delta = 1 + \Sigma_{(2)}R_\delta^2$ and $M_\delta = (4\pi/3)R_\delta^3$. If the mass density near centre Σ_δ are given, then the others are determined by

$$R_\delta = \sqrt{\frac{1 - \Sigma_\delta}{|\Sigma_{(2)}|}} \quad , \quad M_\delta = \frac{4}{3}\pi \left(\frac{1 - \Sigma_\delta}{|\Sigma_{(2)}|} \right)^{3/2}. \quad (\text{A.5})$$

In numerical calculation, we have solved TOV equations (11a) and (11b) for interval $0 < \Sigma \leq \Sigma_\delta$ with initial condition (A.5). Also, we have checked the convergence of numerical solutions with varying Σ_δ . All results in this paper are obtained using $\Sigma_\delta = 1 - 10^{-4}$.

References

- [1] Miyoshi M, Ishitsuka J K, Kamenno S, Shen Z and Horiuchi S 2004 Direct imaging of the massive black hole SgrA* *Prog. Theor. Phys. Suppl.* **155** 186
- [2] Doeleman S S *et al* 2008 Event-horizon-scale structure in the supermassive black hole candidate at the galactic centre *Nature* **455** 78
- [3] Takahashi R 2004 Shapes and positions of black hole shadows in accretion disks and spin parameters of black holes *Astrophys. J.* **611** 996
- [4] Kanai K and Nambu Y 2013 Viewing black holes by waves *Class. Quantum Grav.* **30** 175002
- [5] Sakai N, Saida H and Tamaki T 2014 Gravastar shadows *Phys. Rev. D* **90** 104013
- [6] Fujisawa A, Saida H, Yoo C and Nambu Y 2015 Maximum mass of a barotropic spherical star *Class. Quantum Grav.* submitted (arXiv:1503.01517[gr-qc])
- [7] Nilsson U S and Uggla C 2001 General relativistic stars: polytropic equations of state *Annals Phys.* **286** 292
- [8] Buchdahl H A 1959 General relativistic fluid spheres *Phys. Rev.* **116** 1027
- [9] Barraco D and Hamity V H 2002 Maximum mass of a spherically symmetric isotropic star *Phys. Rev. D* **65** 124028